applied sciences

MDPI

Article

A Low-Hydroxyl Quartz Glass Prepared by Using a Plasma Heat Source as the Flame and High-Purity Quartz Sand as the Raw Material

Xinmin Yu [1,*], Xiurong Du [1,2,*], Xuefu Song [1], Yongchang Zhu [1], Xing Liu [1], Lisheng Zhou [1], Xueyi Zhu [2] and Kai Qiu [2]

[1] China Building Materials Academy, Beijing 100024, China
[2] Laboratory of Science and Technology on Marine Navigation and Control, China State Shipbuilding Corporation, Tianjin 300131, China
* Correspondence: yuxinmin@cbma.com.cn (X.Y.); duxiurong123@126.com (X.D.)

Abstract: In this paper, a quartz glass with low hydroxyl groups was prepared by combining the advantages of various processes, using a plasma heat source as the flame and high-purity quartz sand as the raw material. The purity of the quartz sand was 99.997%. The number of air bubbles in the quartz glass prepared using high-purity quartz sand was lower. The hardness and tensile strength of the quartz glass were 737.7–767.1 GPa and 6.88–9.64 MPa, respectively. The hydroxyl content of the sample was only 4.11 ppm, and the hydroxyl content of the homogenized quartz glass was reduced to 2.64 ppm, which was an improvement of about 35%. After homogenization, the fictive temperature (T_f) of the quartz glass was determined to be 1253 cm^{-1}, and the variation of the T_f value along the radial direction was reduced, indicating a more homogeneous glass structure. The stress distribution in the quartz glass was significantly improved. These results indicate that the preparation of quartz glass from high-purity quartz sand using a plasma heat source as the flame opens up new avenues for optical applications.

Keywords: quartz glass; plasma chemical vapor deposition; hydroxyl; optical homogeneity

Citation: Yu, X.; Du, X.; Song, X.; Zhu, Y.; Liu, X.; Zhou, L.; Zhu, X.; Qiu, K. A Low-Hydroxyl Quartz Glass Prepared by Using a Plasma Heat Source as the Flame and High-Purity Quartz Sand as the Raw Material. *Appl. Sci.* **2024**, *14*, 9137. https://doi.org/10.3390/app14199137

Received: 7 September 2024
Revised: 25 September 2024
Accepted: 3 October 2024
Published: 9 October 2024

1. Introduction

Glass production dates back several millennia, yet it was not until 1813 that Marcet achieved the micro-scale synthesis of quartz glass. Quartz glass, characterized by high hardness, high transmittance, and excellent chemical stability, has become an indispensable material in cutting-edge technologies such as optical devices, biomedical microstructures, space technology, and fiber-optic communications [1–4].

With the rapid advancements in high-purity quartz glass preparation techniques, the primary methods for producing quartz glass include electric melting, gas refinement, chemical vapor deposition (CVD) [5,6], and plasma chemical vapor deposition (PCVD) [7]. The electric melting method utilizes natural crystal or quartz sand as the raw materials, with electric resistance or medium-frequency induction as the heat sources. This method produces quartz glass with a low hydroxyl content and metal impurities, related to the raw material purity, and is commonly used in lighting and crucibles. Zhang [8] et al. prepared quartz glass tubes using the electric melting method, demonstrating that the lowest power consumption was achieved when using 160 kW to melt a 400 mm diameter quartz glass tube. The gas refinement method employs a mixture of hydrogen and oxygen as a heat source to melt the raw materials (natural crystal or quartz sand) into quartz glass. Due to the use of a hydrogen and oxygen mixture as the heat source, this type of quartz glass has a lower economic cost and is often applied in low-grade optical plates and fiber-optic holding rods. Wang et al. [9] successfully prepared Yb^{2+}/Yb^{3+} co-doped quartz glass using the gas refinement method, which exhibited a strong absorption intensity and multiple

absorption peaks, with the absorption spectrum tail extending to longer wavelengths. The CVD method uses $SiCl_4$ or other synthetic silicon compounds as the raw materials, with a mixture of hydrogen and oxygen as the heat source, to synthesize quartz glass through chemical deposition. This type of quartz glass possesses advantages such as high purity, high optical homogeneity, and radiation resistance and is commonly used in the production of precision optical lenses and ultraviolet optical plates. Yuan [10] et al. synthesized graphene superhydrophobic transparent glass using the CVD process, demonstrating adjustable quality for all glass samples, excellent film uniformity, and potential scalability. The PCVD process is employed to fabricate high-purity quartz glass. This method utilizes a plasma flame as a heat source and high-purity $SiCl_4$ as a precursor to produce Type IV quartz glass with the highest purity [11,12]. The quartz glass produced by the PCVD process is characterized by low metal impurities and hydroxyl content, high optical homogeneity, high spectral transmittance, and a wide transmittance range (0.18–3.5 μm), making it an ideal material for specialized optical applications and high-quality quartz materials. However, the PCVD process has the disadvantages of a slower deposition rate and a higher cost, so it cannot be widely used in the field of optical materials.

For quartz glass used in the optical field, there are many factors affecting optical quartz glass, of which the hydroxyl content is particularly important. In terms of physical properties, too much hydroxyl content in optical quartz glass will lead to quartz glass at high temperatures prone to the cracking phenomenon, reducing its mechanical properties. In terms of chemical properties, the hydroxyl group easily controls gas and impurities, thus affecting the chemical stability and corrosion resistance of the quartz glass, in addition to affecting its radiation resistance [13,14]. In terms of optical properties, the presence of the hydroxyl group reduces the light transmission performance and optical purity of the quartz glass and reduces its refractive index. Therefore, the preparation of quartz glass with a low hydroxyl content is particularly important.

Based on the advantages of gas refinement, chemical vapor deposition (CVD) and plasma chemical vapor deposition (PCVD) have been used for the preparation of quartz glass. In this paper, quartz glass with a low hydroxyl content and a low cost was prepared by using high-purity quartz sand as the raw material and a plasma flame as the heat source. The silica network structure and hydroxyl content of the quartz glass were characterized using a Twyman–Green interferometer, UV–Vis–NIR spectroscopy, and infrared reflection spectroscopy.

2. Experimental Section

2.1. Sample Synthesis

In this experiment, a plasma flame was generated in the reactor by means of high-frequency induction, and high-purity quartz sand entered into the reactor through the carrier gas. SiO_2 particles were formed under the high temperature inside the plasma flame, and the SiO_2 particles deposited on the surface of the substrate melted to form quartz glass under the heating effect of the plasma flame. The temperature inside the melting furnace was 3000 °C, and the preparation cycle was 3 days. The prepared quartz glass was transferred to a high-temperature homogenizing oven, kept at a high temperature for 1 h, and then cooled to room temperature to obtain the desired glass samples. The samples were then polished and ground before performance testing. The dimensions of the quartz glass samples obtained were 240 mm in diameter and 200 mm in height. The preparation process is shown in Figure 1. In this paper, two types of quartz sands were selected for testing, labeled as Sample I and Sample II. The sample numbers of the prepared quartz glass are labeled as Samples A–E, respectively.

Figure 1. Process flow diagram.

2.2. Characterizations

The quartz glass melting furnace was designed and manufactured by China Building Materials Academy Co., Ltd., Beijing, China. The high-purity quartz sand was prepared by China Building Materials Academy Co., Ltd. The microscopic morphology of the quartz sand was tested using a LEXT OLS5100 3D laser confocal microscope from OLYMPUS Co., Ltd., Tokyo, Japan. A Shimadzu UV3101-PC UV–Vis–NIR spectrophotometer was used to measure the transmission spectrum of the quartz glass in the range of 190–3200 nm. A PerkinElmer PE1600 Fourier transform infrared spectrophotometer was employed to study the infrared reflection spectrum of the quartz glass, with a measurement range of 400–4000 cm^{-1} and a resolution of 0.5 cm^{-1}. The compressive strength of the quartz glass was measured using a Mach-1 multifunctional 3D indentation machine from BMM. The measurement of the tensile strength of the quartz glass was performed using a WAW-600D electro-hydraulic servo universal testing machine.

3. Results and Discussion

The purity of quartz sand is one of the key factors affecting the quality of quartz glass. The quality of the quartz sand will directly affect the quality of the quartz glass. Therefore, it is especially important to choose a suitable quartz sand. Table 1 shows the impurity content of two kinds of high-purity quartz sand. The SiO_2 content of sample I (99.997%) is higher than that of sample II (99.982%). The content of the alkali metal impurities (Li, Na, and K) of sample I is only 3.77 ppm, and the content of the alkali metal impurities will directly affect the loss of permeability and the thermal stability of the quartz glass. Figure 2 shows the morphology photo of the quartz sand under a laser confocal microscope. The morphology of sample I is lumpy with a similar aspect ratio. The morphology of sample II is mostly long columnar.

Table 1. Content of impurity elements in different types of high-purity quartz sand.

Sample	SiO_2 (%)	Al	B	Ca	Co	Cu	Fe	K	Li	Mg	Mn	Na	Ni	Ti
		μg/g												
I	99.997	17.28	0.04	0.58	<0.01 *	0.02	0.17	0.15	2.32	<0.04 *	<0.01 *	1.43	<0.02 *	1.52
II	99.982	128.6	1.39	0.7	<0.03 *	0.04	0.17	0.92	42.3	<0.08 *	0.14	12.1	<0.03 *	0.07

"*" indicates the minimum range of the test equipment.

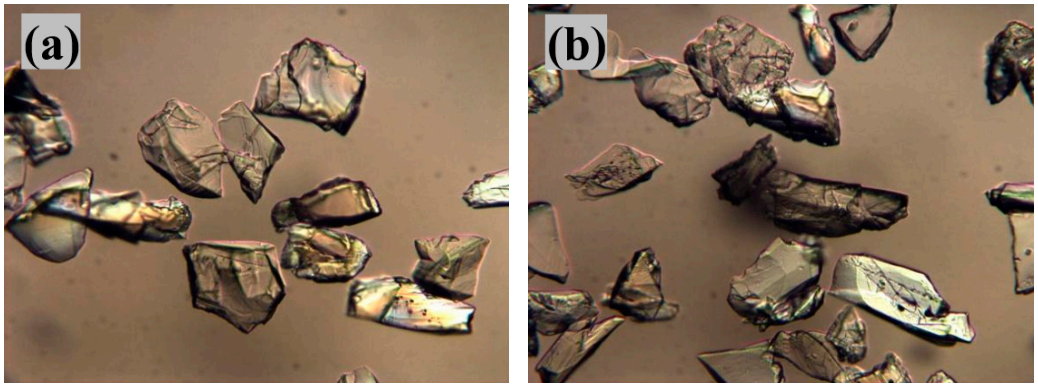

Figure 2. Morphology photos of quartz sand under laser confocal microscope. (**a**) Sample I, and (**b**) Sample II.

Figure 3 shows photographs of the bubble distribution of the quartz glass prepared using different quartz sands. As can be seen from Figure 3, the number of bubbles in the quartz glass prepared from raw material I is smaller than in the quartz glass prepared from raw material II, and the average size of the bubbles is much smaller than in raw material II. The bubble defects in quartz glass due to residual impurities can be greatly reduced because of the lower content of residual impurities in raw material I. Therefore, the high-purity quartz sand of type I was selected as the raw material of the quartz glass.

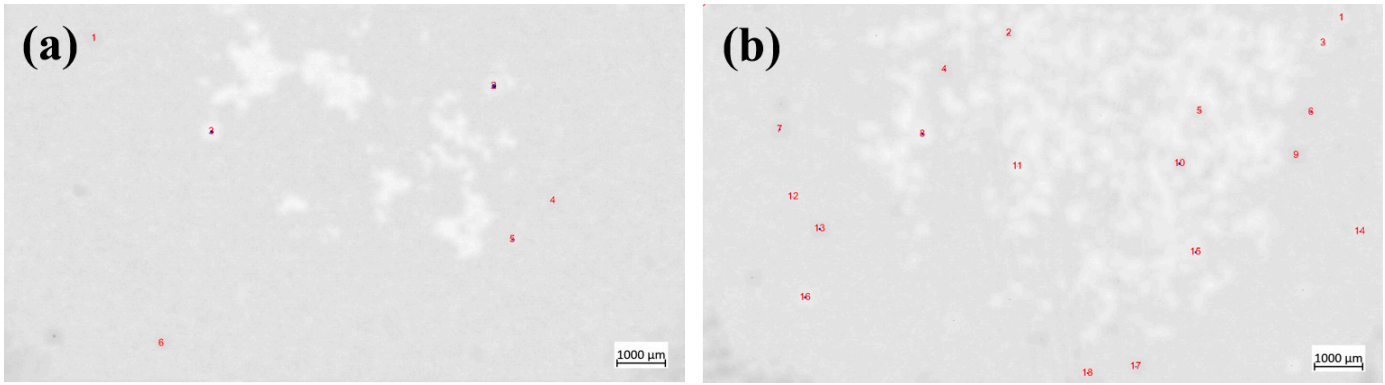

Figure 3. Photographs of the bubble distribution of quartz glass prepared using different quartz sands. (**a**) Sample I, and (**b**) Sample II.

Compressive strength and tensile strength are two important characteristics of quartz glass. The compressive strength of the samples was tested by the indentation method, and the results are shown in Table 2. The compressive strength of the samples was in the range of 737.7~767.1 GPa. The samples were processed to measure the tensile strength, and the dimensional error of the quartz glass processing was ±0.05 mm. The testing instrument recorded the tensile value of each test sample in real time from the beginning of stretching to the occurrence of rupture. In order to minimize the testing error, five samples of quartz glass were tested, and the tensile strength was calculated according to Equation (1).

$$R_m = \frac{F_m}{A} \quad (1)$$

where R_m denotes the tensile strength of the sample; F_m denotes the value of the maximum tensile force corresponding to the occurrence of a fracture in the sample; and A denotes the cross-sectional area of the fracture zone. The tensile strength of the samples was 6.88~9.64 MPa, only one-seventieth of the compressive strength, which is consistent with the general results for materials such as glass and ceramics, i.e., compressive strength is much greater than tensile strength. According to previous studies [15], quartz glass belongs

to a group of typical brittle materials, with little toughness, low plasticity, and a poor ductility ability, so a brittle fracture occurs under a very small tensile force; however, quartz glass has large hardness and good stiffness, so it has a strong compressive ability.

Table 2. Compressive strength and tensile strength of quartz glass.

	Sample A	Sample B	Sample C	Sample D	Sample E
Compressive strength (GPa)	754.8 ± 0.6	735.7 ± 0.7	737.7 ± 0.9	738.2 ± 0.4	767.1 ± 0.6
Tensile strength (MPa)	8.15 ± 0.2	8.41 ± 0.4	8.19 ± 0.3	9.64 ± 0.6	7.93 ± 0.3

The density of quartz glass is an important parameter, which is closely related to the quality, performance, and application of quartz glass. Normally, the density of optically transparent quartz glass is 2.20–2.21 g/cm^3, and the density of opaque quartz glass is smaller, about 2.02–2.10 g/cm^3. In this experiment, the drainage method was used to determine the density of the quartz glass. The quartz glass sample with a diameter of 0.1 mm wire was suspended in the analytical electronic balance in the air and water, weighing the quartz glass, and, finally, Equation (2) was used to calculate the density of the quartz glass.

$$d = \frac{m_1 - m_1}{(m_1 - m_1) - (m_1 - m_1)} \times (\rho - 0.0012) + 0.0012 \quad (2)$$

where m_1 represents the total weight of the quartz glass sample and metal wire in air, m_2 denotes the weight of the metal wire in air, m_3 indicates the total weight of the quartz glass sample and metal wire in water, and m_4 signifies the weight of the metal wire in water. The density of water is represented by ρ, while 0.0012 g/cm^3 is the average density of air at room temperature. To minimize experimental data errors, the sample was tested five times, as illustrated in Figure 4. The quartz glass densities obtained from these five tests were 2.208 g/cm^3, 2.213 g/cm^3, 2.197 g/cm^3, 2.198 g/cm^3, and 2.209 g/cm^3, with a margin of error of ±0.003. The average density was calculated to be 2.205 g/cm^3.

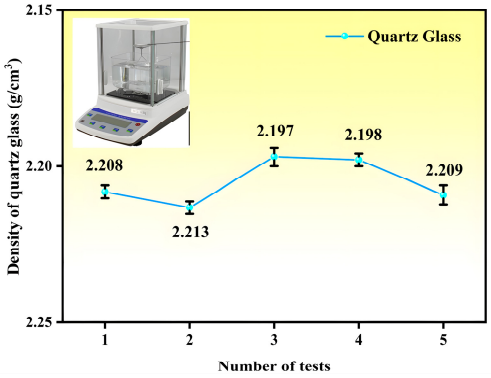

Figure 4. Density of quartz glass.

Fictive temperature (T_f) is a crucial parameter for characterizing the structure of quartz glass. The concept of "fictive temperature" was first proposed by Tool et al. [16] in the 1940s, who suggested that this parameter could represent the structural state of glass. If the structure of glass in a certain state is identical to the equilibrium structure at temperature T, the fictive temperature of that glass state can be considered as $T_f = T$ [17]. In other words, when quartz glass reaches equilibrium at temperature T and is suddenly cooled to room temperature, its fictive temperature is T. Agrawal et al. [18] found that infrared spectroscopy can be used to characterize the imaginary temperature of the quartz glass. Figure 5 displays the infrared reflection spectrum of quartz glass from 300 to 1600 cm^{-1}, featuring three characteristic vibration bands at 1122, 780, and 480 cm^{-1}, consistent with the measurements by Agarwal et al. The 480 cm^{-1} band corresponds to the Si–O–Si rocking

vibrations, while the 780 cm^{-1} spectral band is attributed to the Si–O–Si bending vibrations. According to the literature, the 1122 cm^{-1} band is ascribed to the Si–O–Si bond stretching vibrations, with the position of this reflection band primarily determined by the Si–O–Si bond angle. Notably, the position of the 1122 cm^{-1} band is related to the fictive temperature (T_f). As shown in Figure 5, after the peak deconvolution of the 1122 cm^{-1} band using a Gaussian function, the radial fictive temperature (T_f) of the glass sample was calculated using Equation (3) to characterize the structural changes in the quartz glass [19].

$$v_1 = 1114.5 + (11603.51/T_f) \quad (3)$$

where v_1 represents the measurement position of the 1122 cm^{-1} spectral band with an error value of ±0.3. T_f = 1253 cm^{-1} is obtained according to Equation (3). The calculated T_f value was 1253 K. Figure 6 illustrates the variation of the T_f values along the radial direction before and after homogenization (with a test point position at 40 mm). As depicted in Figure 6, for homogenized quartz glass, T_f values at the edge are higher than those at the center, attributed to the higher cooling rate at the edge compared to the center during the cooling process after a high-temperature homogenization. However, the differences in the fictive temperatures at various radial positions of the homogenized quartz glass are relatively small, indicating a more uniform structure throughout the quartz glass. This uniformity is also related to the distribution state of hydroxyl groups and their impact on structural relaxation.

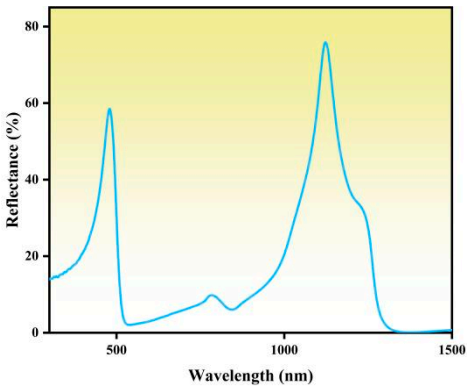

Figure 5. Infrared reflectance spectra of quartz glass.

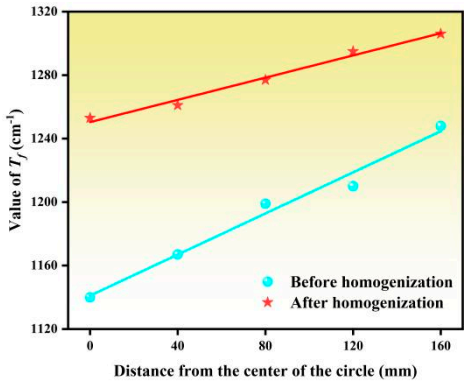

Figure 6. Value of T_f along radius of quartz glass before and after homogenization.

For optical quartz glass, hydroxyl groups disrupt the integrity of the silica network structure, leading to an increase in the "non-bridging oxygen" content and greater disorder in the silica network. An uneven distribution of hydroxyl content within quartz glass can result in anisotropy, affecting light refraction and absorption when passing through these local regions, manifesting as differences in optical homogeneity in test results. Therefore, to improve the optical homogeneity of the glass, hydroxyl groups must be uniformly

distributed in the vertical plane through which light passes. The hydroxyl content of samples can be measured using the transmission spectrum of quartz glass. The hydroxyl content in quartz glass can be calculated using the hydroxyl absorption peak at a 2730 nm wavelength according to Equation (4) [20]:

$$C = 96.5\frac{1}{d}\log(\frac{I_0}{I}) \quad (4)$$

where C is the hydroxyl content in the sample (ppm) with an error of ± 0.02, d is the sample thickness (mm), I_0 is the distance from the baseline to the zero line at 2730 nm (mm), and I is the distance from the absorption peak to the zero line at 2730 nm (mm). Figure 7 shows the UV–visible transmission spectra of the quartz glass before and after homogenization. Using Equation (4), it can be seen that the hydroxyl content of the quartz glass prepared in this experiment was only 4.11 ppm, and the hydroxyl content of the quartz glass prepared by the CVD process was 1108 ppm. According to the literature, the hydroxyl content of quartz glass prepared by the CVD method is 880 ppm according to Jia et al. [21] and 1200 ppm according to Sato et al. [22]. Comprehensively, the hydroxyl content of the quartz glass prepared in this paper is much lower than that from the CVD process, which may be due to the difference in the heat source of the preparation process. The CVD process uses hydrogen and oxygen as the heat source, and the reaction between the hydrogen and oxygen generates water, so that the hydroxyl group of the quartz glass prepared by the CVD process has a high content of the hydroxyl group. In addition, the hydroxyl content before homogenization was 4.11 ppm, and, after homogenization, it decreased to 2.64 ppm. The homogeneity improved significantly by 35% after the high-temperature treatment. According to the water molecule diffusion reaction Equation (5) and the diffusion rate Equation (6), during high-temperature homogenization [23–26], D denotes the diffusion coefficient of water and $\partial C/\partial X$ denotes the concentration gradient of water. The relationship between the diffusion coefficient D and temperature T is LnD~1/T, which is linear. At high temperatures, water diffuses more readily from high to low concentrations, promoting a uniform hydroxyl distribution in the glass. Simultaneously, during high-temperature vacuum pressure tank homogenization, the glass flow facilitates the physical migration and homogenization of the hydroxyl groups.

$$H_2O + \equiv Si - O - Si \equiv \rightleftarrows \equiv SiOH + \equiv SiOH \quad (5)$$

$$J = -D(\partial C/\partial X) \quad (6)$$

Figure 8 shows the radial variation of the hydroxyl content in the quartz glass after homogenization. As shown in Figure 8, the hydroxyl content in this sample shows an increasing trend from the center to the edge, which may be due to the different atmospheres at various places near the deposition surface during the deposition process, which, in turn, causes the uneven distribution of hydroxyl groups.

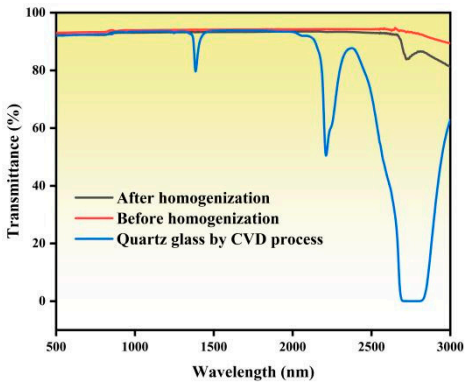

Figure 7. The UV–visible transmission spectra of quartz glass before and after homogenization.

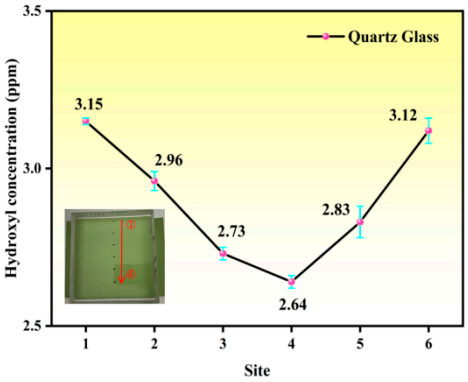

Figure 8. Plot of the distribution of hydroxyl groups in quartz glass after homogenization; the inset shows the location of the pickup points.

Figure 9 compares the stress interference color patterns of quartz glass samples before and after homogenization. Figure 9a shows circular stress patterns before homogenization, with alternating blue and orange colors at equal distances from the sample center, divided into four quadrants. This phenomenon occurs because in quadrants I and III, the total optical path difference δ equals the sum of the polarizing stress meter's full glass plate optical path difference δ_0 and the glass optical path difference δ_g. In quadrants II and IV, the total optical range difference δ is the difference between the polarimeter's full slide optical range difference δ_0 and the quartz glass optical range difference δ_g. Consequently, the stress interference color sequences are opposite. When glass exhibits compressive stress, $\delta_0 < 0$; when tensile stress is present, $\delta_0 > 0$. Therefore, in the first quadrant, the compressive stress interference colors precede purple-red (e.g., yellow, orange, and red), while the tensile stress interference colors follow purple-red (e.g., blue, green, and yellow-green). Figure 9a shows alternating orange–blue–orange interference colors in the first quadrant, indicating alternating a compressive–tensile–compressive circular stress distribution. Figure 9b displays the stress interference color pattern after annealing, showing an overall purple-red color, indicating a significant stress improvement.

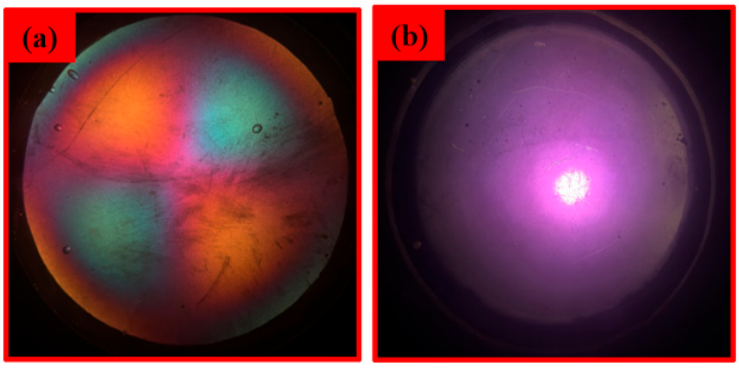

Figure 9. Stress photographs of quartz glass before and after homogenization. (**a**) Before homogenization, and (**b**) after homogenization.

4. Conclusions

A plasma heat source was used as the flame and high-purity quartz sand was used as the raw material to prepare quartz glass. The purity of the quartz sand was measured to be 99.997%. Under the microscope, the morphology of the quartz sand was mostly lumpy with a similar length and width. The number of air bubbles in the prepared quartz glass was low. The hardness and tensile strength of the quartz glass were 737.7–767.1 GPa and 6.88–9.64 MPa, only one-seventieth of the hardness, which was consistent with the general results of hard and brittle materials such as glass and ceramics, i.e., compressive strength is much greater than tensile strength. This was mainly due to the different choice of heat

source. The CVD process uses hydrogen and oxygen as the heat source, which generates water during the reaction process, leading to a high hydroxyl content in the quartz glass. After homogenization, the assumed temperature of the quartz glass was determined to be 1253 cm^{-1} and the variation of the T_f value along the radial direction decreased, indicating a more homogeneous glass structure. The hydroxyl content of the sample was only 4.11 ppm, which was much lower than that of the quartz glass prepared with the CVD process. After homogenization, the hydroxyl content was reduced to 2.64 ppm, which was a significant improvement of about 35%. Moreover, the hydroxyl content of the samples tended to increase from the center to the edge. A comparison of the stress interference color sequence diagrams before and after homogenization shows that the stress of the homogenized quartz glass was significantly improved. These results indicate the potential application of this quartz glass in the optical field.

Author Contributions: Conceptualization, X.Y. and X.D.; methodology, X.Y. and X.S.; software, X.Y. and X.L.; validation, X.Y. and L.Z.; formal analysis, X.Y. and X.D.; investigation, X.Z. and K.Q.; resources, Y.Z. and X.D.; data curation, X.Y. and X.S.; writing—original draft preparation, X.Y.; writing—review and editing, X.S.; visualization, X.D.; supervision, X.D.; project administration, Y.Z.; funding acquisition, X.D. and Y.Z. All authors have read and agreed to the published version of the manuscript.

Funding: This research is supported by Laboratory of Science and Technology on Marine Navigation and Control, China State Shipbuilding Corporation, Project 2023010202.

Institutional Review Board Statement: Not applicable.

Informed Consent Statement: Not applicable.

Data Availability Statement: Data is contained within the article.

Conflicts of Interest: Authors Xiurong Du, Xueyi Zhu and Kai Qiu were employed by the company China State Shipbuilding Corporation. The remaining authors declare that the research was conducted in the absence of any commercial or financial relationships that could be construed as a potential conflict of interest.

References

1. Ovchinnikov, S.V.; Sergeev, V.P.; Kalashnikov, M.P. Studying the Ultimate Strength and Service Life of Quartz Glass with Protective Coating for Space Vehicle Windows. *Russ. Phys. J.* **2024**, *67*, 307–314. [CrossRef]
2. Qian, Y.G.; Shen, Y.C.; Sun, F.; Chen, J.J.; Tang, M.M.; Chen, F.; Chen, Y.L.; Sun, Y.J.; Shen, H.P. Improving the UV transmittance of synthetic quartz through defect repair methods. *J. Non-Cryst. Solids* **2024**, *635*, 123019. [CrossRef]
3. Gawel, B.A.; Busam, J.; Marthinsen, A. Influence of aluminium doping on high purity quartz glass properties. *RSC Adv.* **2024**, *14*, 13669–13675. [CrossRef] [PubMed]
4. Shi, M.; Zhang, M.M.; Wang, L. Temperature control of atomic gas chamber using a nonmagnetic heating chip fabricated on quartz substrate. *Eur. Phys. J.-Appl. Phys.* **2024**, *99*, 12. [CrossRef]
5. Tandon, P.; Rosner, D.E. Codeposition on Hot CVD Surfaces: Particle Dynamics and Deposit Roughness Interactions. *AIChE J.* **1996**, *42*, 1673–1684. [CrossRef]
6. Xu, C.; Wang, Y.J.; Shu, Z.M.; Song, X.F.; Wang, L. Effect of the Silica Glass Ingot Surface Morphology on the Synthetic Deposition Rate by CVD Method. *J. Wuhan Univ. Technol.* **2010**, *32*, 119–122.
7. Song, X.F.; Sun, Y.C.; Du, X.R.; Zhang, X.Q.; Hua, N.; Li, H.Y. Process of PCVD Synthesize Hyper Pure Silica Glass. *Bull. Chin. Ceram. Soc.* **2017**, *36*, 43–46.
8. Zhang, S.X.; Zhang, S.B.; Wang, Y.M. Centrifugation and Fusion Process for Opaque Large-bore Quartz Glass Tube. *Bull. Chin. Ceram. Soc.* **2011**, *30*, 534–537.
9. Wang, C. Study on Preparation of Yb^{2+}/Yb^{3+} Co-Doped Silica Glass Based on Flame Fusion Process and Spectroscopic Characteristics. *Chin. J. Lumin* **2017**, *38*, 32–36. [CrossRef]
10. Yuan, Y.W.; Wang, Y.S.; Liu, S.S.; Zhang, X.X.; Liu, X.Z.; Sun, C.H.; Yuan, D.; Zhang, Y.; Cao, X.R. Direct chemical vapor deposition synthesis of graphene super-hydrophobic transparent glass. *Vacuum* **2022**, *202*, 111136. [CrossRef]
11. Song, X.F.; Sun, Y.C.; Zhong, H.; Wang, H.J.; Gu, Z.A. Synthesis of Silica Glass by Plasma Chemical Vapor Deposition Method. *J. Chin. Ceram. Soc.* **2008**, *36*, 531–534.
12. Nie, L.J.; Wang, Y.F.; Xiang, Z.K.; Wang, L.; Wang, H. Preparation and application of high-performance synthetic optical fused silica glass. *Opt. Precis. Eng.* **2016**, *24*, 2916–2924.

13. Trukhin, A.N.; Fitting, H.-J. Investigation of optical and radiation properties of oxygen defcient silica glasses. *J. Non-Cryst. Solids* **1999**, *248*, 49–64. [CrossRef]
14. Borovkova, L.B.; Popov, O.N.; Belyakov, A.V.; Savitskas, R.K.; Teplov, G.S. Corrosion Resistance of Heat Resistant Materials Based on Quartz glass. *Glass Ceram.* **1980**, *6*, 14–15. [CrossRef]
15. Sun, Y.C.; Song, X.F.; Zhang, X.Q.; Du, X.R. Silica Glass for Inertial Navigation System. *Navig. Control* **2019**, *18*, 1–48.
16. Tool, A.Q. Relation Between Inelastic Deformability and Thermal Expansion of Glass in Its Annealing Range. *J. Am. Ceram. Soc.* **1964**, *29*, 240–253. [CrossRef]
17. Zhang, T.H.; Zhao, L.J.; Cheng, J.; Yin, Z.Y.; Li, T.Y.; Chen, M.J.; Li, W.; Yuan, X.D. Role of fictive temperature distribution involved in CO_2 laser polishing of fused silica and its optimization for achieving even heat-affected zones. *Appl. Surf. Sci.* **2024**, *670*, 160605. [CrossRef]
18. Agarwal, A.; Davis, K.M.; Tomozawa, M. A Simple IR Spectroscopic Method for Determining Fictive Temperature of Silica Glass. *J. Non-Cryst. Solids* **1995**, *185*, 191–198. [CrossRef]
19. Liao, W.; Zhang, C.C.; Chen, J.; Yang, K.; Zhang, L.J.; Jiang, X.L.; Bai, Y.; Wamg, H.J.; Luan, X.Y.; Jiang, X.D. Evolution Regularity of Continuous Surface Structures Shaped by Laser-Supported Fictive-Temperature Modifying. *Crystals* **2023**, *13*, 542. [CrossRef]
20. Kuzuu, N.; Horikoshi, H.; Okazaki, A.; Seki, T.; Tanaka, M. Hydroxyl-concentration distribution near the binding interface formed by heating contacted flat silica glass surfaces at high temperature. *J. Ceram. Soc. Jpn.* **2009**, *117*, 211–213. [CrossRef]
21. Jia, Y.N.; Wang, Y.F.; Nie, L.J.; Xiang, Z.K.; Wang, L.; Liu, F.X.; Rao, C.D. Test and Analysis of Hydroxyl Group in CVD Synthetic Silica Glass. *Key Eng. Mater.* **2017**, *726*, 419–423. [CrossRef]
22. Sato, N.; Yamamotol, T.; Kuzuul, N.; Horikoshi, H.; Niwa, S. Diffusion of hydroxyl groups in silica glass through the binding interface. *Jpn. J. Appl. Phys.* **2016**, *55*, 02BC13. [CrossRef]
23. Xiang, Z.K.; Wang, Y.J.; Wang, Y.F. Influence of trough sedimentation on the optical homogeneity of synthetic quartz glass. *China Build. Mater. Sci. Technol.* **2000**, *1*, 35–36.
24. Davis, M.; Agarwal, A.; Tomozawa, M.; Hirao, H. Quantitative infrared spectroscopic measurement of hydroxyl concentrations in silica glass. *J. Non-Cryst. Solids* **1996**, *203*, 27–36. [CrossRef]
25. Davis, M.; Tomozawa, M. An infrared spectroscopic study of water-related species in silica glasses. *J. Non-Cryst. Solids* **1996**, *201*, 177–198. [CrossRef]
26. Nobu, M.Z.; Naoya, S.; Yu, A.; Horikoshi, H.; Horii, N. Temperature and hydroxyl concentration dependences of diffusion coefficients of hydroxyl groups in vitreous silica at temperatures of 850–1200 °C. *Jpn. J. Appl. Phys.* **2017**, *56*, 111303.